A new concept multi-stage Zeeman decelerator: experimental implementation

Theo Cremers, Simon Chefdeville, Niek Janssen, Edwin Sweers,
Sven Koot, Peter Claus, and Sebastiaan Y.T. van de Meerakker*
Radboud University, Institute for Molecules and Materials,
Heijendaalseweg 135, 6525 AJ Nijmegen, the Netherlands
(Dated: December 3, 2024)

We demonstrate the successful experimental implementation of a multi-stage Zeeman decelerator utilizing the new concept described in the accompanying paper. The decelerator consists of an array of 25 hexapoles and 24 solenoids. The performance of the decelerator in acceleration, deceleration and guiding modes is characterized using beams of metastable Helium (^3S) atoms. Up to 60% of the kinetic energy was removed for He atoms that have an initial velocity of 520 m/s. The hexapoles consist of permanent magnets, whereas the solenoids are produced from a single hollow copper capillary through which cooling liquid is passed. The solenoid design allows for excellent thermal properties, and enables the use of readily available and cheap electronics components to pulse high currents through the solenoids. The Zeeman decelerator demonstrated here is mechanically easy to build, can be operated with cost-effective electronics, and can run at repetition rates up to 10 Hz.

PACS numbers: 37.10.Mn, 37.20.+j

I. INTRODUCTION

In the accompanying paper we proposed a new concept multi-stage Zeeman decelerator, consisting of an alternating array of deceleration solenoids and focusing hexapoles, that is specifically optimized for crossed beam scattering experiments. The hexapoles are introduced as a focusing element to counteract the inherent defocusing forces of the solenoid fringe fields [1, 2], resulting in a significant improvement of the decelerator's performance. Here, we present the successful experimental implementation of the concept, using a relatively short proof-of-concept decelerator consisting of 24 solenoids and 25 hexapoles. The performance of the decelerator in both deceleration, acceleration and guiding modes is studied by passing a beam of metastable He (^3S) atoms through the decelerator. We chose metastable He as this system has frequently been used to test and characterize new decelerator designs [3, 4]. The recorded time-of-flight profiles of atoms exiting the decelerator show excellent agreement with the results from numerical trajectory simulations, verifying that the multi-stage Zeeman decelerator exhibits phase stable operation.

An essential part in a multi-stage Zeeman decelerator is the design of the deceleration solenoids, and the cooling strategy to remove the dissipated energy. A variety of solenoid designs have been implemented successfully in multi-stage Zeeman decelerators before. Merkt and coworkers utilized tightly-wound solenoids of insulated copper wire that were thermally connected to water-cooled ceramics [5]. Later, similar solenoids were placed outside a vacuum tube, and submerged in a bath of cooling water [6]. This improved the cooling capacity, and enabled the experiment to operate at repetition rates of 10 Hz. Raizen and coworkers also developed a multi-stage Zeeman decelerator, referred to as the atomic or molecular coilgun, that is based on solenoids encased in high permeability material to increase the on-axis maximum magnetic field strength [7, 8]. Recently, different types of traveling wave Zeeman decelerators have been developed, which consists of numerous spatially overlapping quadrupole solenoids [9], or a helical wire arrangement to produce the desired magnetic field [10].

In the decelerator presented here, we use a new type of solenoid that is placed inside vacuum, but that allows for direct contact of the solenoid material with cooling liquid. The solenoid design offers excellent thermal properties and allows for the use of low-voltage electronic components that are readily available and cost effective. Together, this results in a multi-stage Zeeman decelerator that is relatively easy and cheap to build, and that can be operated at repetition rates up to 10 Hz.

This paper is organized as follows. In section II we describe in detail the experimental setup, focusing mainly on the technical details of the solenoids and hexapoles, together with the driving electronics and cooling system. In section III we present experimental results for the deceleration, acceleration, or guiding of a beam of metastable He atoms, and compare the results to three-dimensional numerical trajectory simulations. Finally, we discuss the future prospects for a longer version of the decelerator that is technically capable of operating at repetition rates up to 30 Hz.

Throughout this paper, we will use the same nomenclature and labeling of parameters as introduced in the accompanying paper.

* basvdm@science.ru.nl

II. EXPERIMENTAL SETUP

A. Multi-stage Zeeman decelerator

An overview of the experiment is shown in Figure 1. The generation and detection of the metastable He beam will be discussed in section II B; in this section we will first describe the decelerator itself, starting with a description of the solenoids and associated electronics.

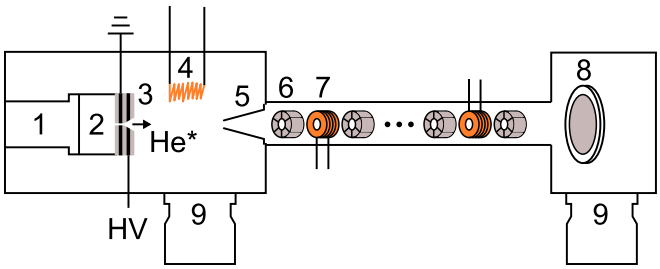

Figure 1. Schematic representation of the experimental setup. The main components are: 1, coldhead; 2, Even-Lavie valve; 3, pinhole discharge; 4, hot filament; 5, skimmer; 6, hexapole; 7, solenoid; 8, MCP detector; 9, turbo-molecular pump

The solenoids consist of 4 windings of a copper capillary that is wound around a 3 mm bore diameter. The capillary has an inner diameter of 0.6 mm and an outer diameter of 1.5 mm, and cooling liquid is circulated directly through the capillary. The solenoid is wound such that the first and last windings end with a straight section of the capillary, as is shown in a photograph of a single solenoid in Figure 2*b*. These straight sections are glued into an aluminum mounting flange, as will be further discussed later.

The use of a single layer of rather thick copper capillary as solenoid material in a Zeeman decelerator is unconventional, but it has some definite advantages. Because of the low-resistance copper capillary, small operating voltages (24 V) are sufficient to generate currents of approximately 4.5 kA that produce a maximum field of 2.2 T on the solenoid axis. This in turn allows for the use of FET-based electronics components to switch these currents, which are considerably cheaper than their high voltage IGBT-based counterparts. The same holds for the power supplies that deliver the current. By running cooling liquid directly through the solenoid capillary, the solenoids are efficiently cooled. The low operation voltage ensures that the cooling liquid does not conduct any significant electricity.

The current pulses are provided by specially designed circuit boards; one such board is displayed in Figure 3*b*. Each solenoid is connected to a single board, that is mounted directly onto the solenoid-flange feedthroughs in order to minimize power loss between board and solenoid. Brass strips are used to mechanically clamp the board to the capillary material. The simplified electronic circuit is shown schematically in Figure 3*a*. The circuit board is mostly occupied by a parallel array of capacitors, with a total capacitance of 70 mF. The capacitors are charged by a 24 V power supply and then discharged through the connected solenoid. The solenoids have a very low resistance R_C of about 1 mΩ and self-inductance L_C of about 50 nH, even compared to the electronic circuit itself. The capacitors are discharged via two possible pathways indicated in red and green, respectively, by activating the two independent gates S1 and S2. Closing gate S1 will allow electrons to flow through the solenoid, generating a maximum current of about 4.5 kA. Closing gate S2 will send the flow through both the solenoid and a 100 mΩ resistor that limits the current to about 150 A. When both gates are opened any remaining power in the solenoid will either dissipate in the electrical components along pathway 3 (in blue) or return to the capacitors. The electronic configuration is able to apply up to two consecutive pulses to each solenoid, as is required for the hybrid mode of operation.

As an example, the current profiles for a single pulse or double pulse are shown in Figure 3*c* and 3*d*, respectively, together with the trigger pulses that activate gates S1 and S2. These profiles were obtained from the induced voltage over a miniature solenoid that was placed inside the center of a decelerating solenoid [11]. The current pulse is initiated by closing gate S1, after which the solenoid current shows a rapid rise to a maximal current of approximately 4.5 kA. After reopening gate S1, the current exponentially decreases with a time constant of 10 μs. Gate S2 is programmed to close automatically for a fixed duration of 50 μs, starting 30 μs after the reopening of S1. While gate S2 is closed, a low-level lingering current is maintained in the solenoid, providing a quantization field for atoms or molecules that are near the solenoid. This field is used to prevent Majorana transitions, as discussed in the accompanying paper.

The solenoids and electronics boards are actively cooled using a closed-cycle cooling system using racing automobile cooling liquid. An approximately 10 cm long capillary section is soldered onto each electronics board, and each capillary is connected in series to its connecting solenoid using silicon tubes. All board-solenoid pairs are individually connected to a mains and return cooling line, using the same flexible silicon material. Each electronics board is additionally cooled by a small fan. Using this cooling system, relatively low operation temperatures are maintained despite the high currents that are passed through the solenoid. In the experiments shown here, the Zeeman decelerator is routinely operated with a repetition frequency of 10 Hz, while the temperature of the solenoids is kept below 40 degrees Celsius.

The solenoids are pulsed in a predefined time sequence designed to control the longitudinal velocity of a specific para-magnetic particle. This time sequence is calculated while taking current profiles into account that are modeled after the measured profiles shown in Figure 3*b*. The resulting pulse sequence for gates S1 and S2 is programmed into a pattern generator (Spincore PulseBlaster PB24-100-4k), which sends pulse signals to each individ-

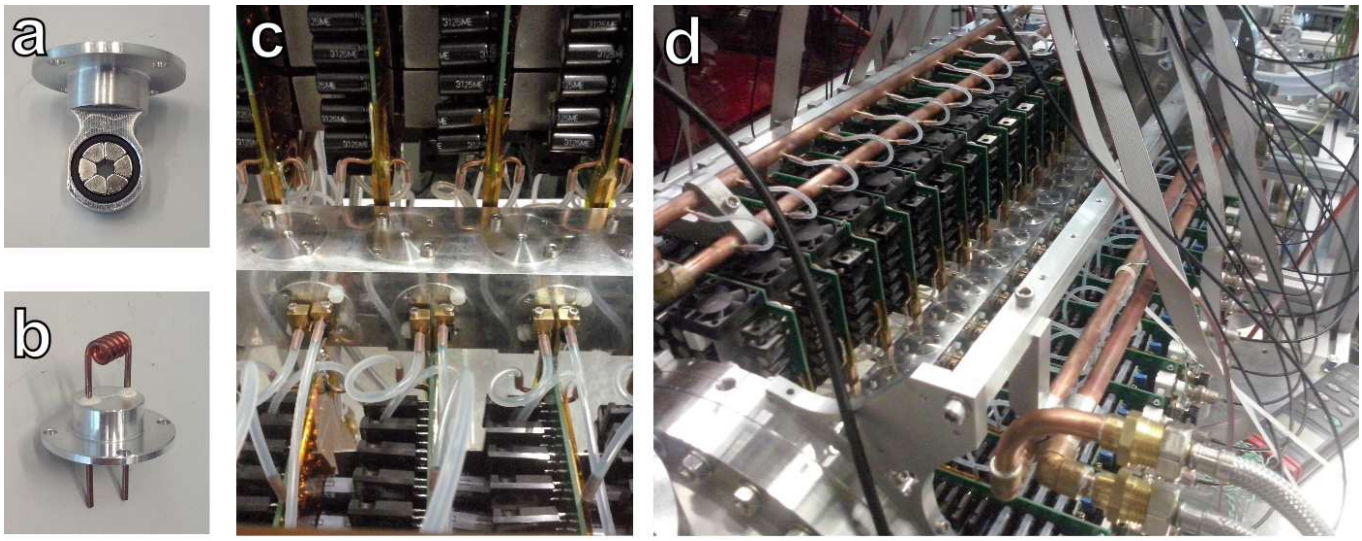

Figure 2. Photographs of the Zeeman decelerator and the most relevant components. (*a*) a hexapole element embedded in a custom flange; (*b*) a solenoid element with connections through a custom flange; (*c*) close-up of the decelerator housing; (*d*) an overview of the decelerator.

ual circuit board. The temperature of each solenoid is continuously monitored via a thermocouple on the connecting clamps of the circuit board. When the temperature of the solenoid exceeds a user-set threshold, operation of the decelerator is interrupted.

The magnetic hexapoles consist of six wedge-shaped permanent magnets in a ring, as seen in Figure 2*a*. Adjacent magnets in the ring have opposite radial magnetization. The inner diameter of the hexapole is 3 mm and the length is 8 mm, such that these dimensions match approximately to the corresponding solenoid dimensions. The magnets used in this experiment are based on NdFeB (grade N42SH) with a remanence of approximately 450 mT. The advantage of using hexapoles consisting of permanent magnets is twofold: first, implementation is mechanically straightforward, and second, no additional electronics are needed to generate the focusing fields. However, this approach lacks any tunability of the field strength. This can in part be overcome by selectively removing hexapoles from the decelerator, or by exchanging the magnets for ones with a different magnetization. If required, electromagnetic hexapoles that allow for tunability of the field strength can be used instead. We have built and successfully operated hexapoles that are made of the solenoid capillary material, and could optimize their focusing strength by simply adjusting the time these hexapoles are switched on. However, we found that similar beam densities were achieved using the permanent hexapoles, and experiments with electromagnetic hexapoles are not further discussed here.

The decelerator contains 24 solenoids and 25 hexapoles that are placed with a center-to-center distance of 11 mm inside a vacuum chamber. The chamber consist of a hollow aluminum block of length 600 mm with a squared cross section of side lengths 40 mm. This chamber is made by machining the sides of standard aluminum pipe material with an inner diameter of 20 mm. Solenoids and hexapoles are mounted on separate flanges, as can be seen in Figure 2, such that each element can be installed or removed separately. The first and last element of the decelerator is a hexapole to provide transverse focusing forces at the entrance and exit of the decelerator, respectively. Openings for the individual flanges on the decelerator housing spiral along the sides between subsequent elements, with clockwise 90 degree rotations. In this way there is enough space on each side of the decelerator to accommodate the electronics boards of the solenoids, which have a 42 mm height. In addition, since subsequent solenoids are rotated by 180 degrees in the decelerator, any asymmetry in the magnetic field because of the relatively coarse winding geometry is compensated.

Vacuum inside the decelerator housing is maintained by a vacuum pump installed under the detection chamber, which has an open connection to the decelerator housing. Only a minor pressure increase in the chamber is observed if the solenoids are operational, reflecting the relatively low operational temperature of the solenoids. Although for longer decelerators additional pumping capacity inside the decelerator is advantageous, we find that for the relatively short decelerator used here the beam density is hardly deteriorated by collisions with background gas provided the repetition rate of the experiment is below 5 Hz.

B. Metastable helium beam

A beam of helium in the metastable $(1s)(2s)\ ^3S$ ($m_S = 1$) state (from this point He*) was used to test the performance of the Zeeman decelerator. This species was

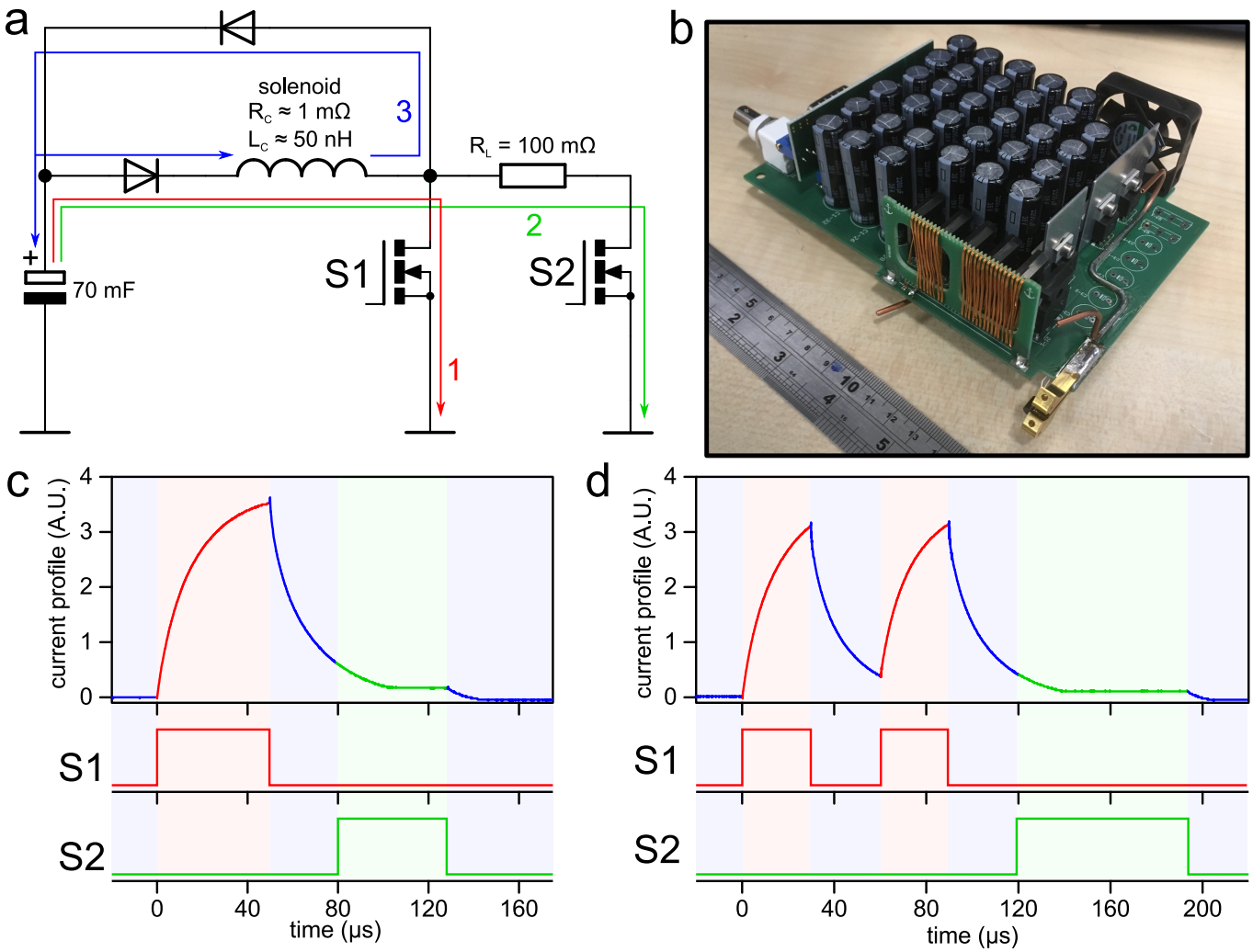

Figure 3. Schematic representation of the driving electronics and the current pulse through a solenoid. (*a*) a schematic drawing of the electronic circuit enabling the solenoid current. The colored pathways correspond to: 1 (red) maximum current through solenoid, 2 (green) reduced current through solenoid, and 3 (blue) dissipation of any leftover current in the solenoid. *b* Photograph of a circuit board driving an individual coil. Current profile of a single (*c*) or double (*d*) pulse through the solenoid derived from the voltage induced in a smaller pickup solenoid. The color coding in the profile indicates the electronic pathway in (a). The trigger pulses for gates S1 and S2 to generate these pulses are shown underneath the current profiles.

chosen for two main reasons. First, He* has a high magnetic moment to mass ratio (2.0 a.u./μ_B/) with a large Zeeman shift, which allows for effective manipulation of the atom with magnetic fields. This allows us to significantly vary the mean velocity of the beam despite the relatively low number of solenoids. Second, He* can be measured directly with a micro-channel plate (MCP) detector, without the need for an ionizing laser, such that full time-of-flight (TOF) profiles can be recorded in a single shot. This allows for a real-time view of TOF profiles when settings of the decelerator are changed, and greatly facilitates optimization procedures.

The beam of He* is generated by expanding a pulse of neat He atoms into vacuum using a modified Even-Lavie valve (ELV) [12] that is cooled to about 16 K using a commercially available cold-head (Oerlikon Leybold). At this temperature the mean thermal velocity of helium is about 460 m/s. The ELV nozzle is replaced by a discharge source consisting of alternating isolated and conducting plates, similar to the source described by Ploenes *et al.* [13]. The discharge occurs between the conducting plates, where the front plate is kept at -600 V and the back plate is grounded. To ignite the discharge, a hot filament running 3 A of current is used. The voltage applied to the front plate is pulsed (20-30 μs duration) to reduce the total energy dissipation in the discharge. Under optimal conditions, a beam of He* is formed, with a mean velocity just above 500 m/s. Unless states otherwise, in the experiments presented here, the decelerator is programmed to select a packet of He* with an initial velocity of 520 m/s.

The beam of He* passes through a 3 mm diameter

skimmer (Beam Dynamics, model 50.8) into the decelerator housing. The first element (a hexapole) is positioned about 70 mm behind the skimmer orifice. The beam is detected by an MCP detector that is positioned 128 mm downstream from the exit of the decelerator. This MCP is used to directly record the integrated signal from the impinging He* atoms.

III. RESULTS AND DISCUSSION

A. Longitudinal velocity control

As explained in the accompanying paper, the decelerator can be operated in three distinct modes of operation: in deceleration or acceleration modes, the atoms are most efficiently decelerated or accelerated, respectively. In the so-called hybrid mode of operation, the beam can be transported or guided through the decelerator at constant speed (some mild deceleration or acceleration is in principle also possible in this mode). In this section, we present experimental results for all three modes of operation.

We will start with the regular deceleration mode. In Figure 4, TOF profiles for He* atoms exiting the decelerator are shown that are obtained when the decelerator is operated in deceleration mode, using different values for the equilibrium phase angle ϕ_0. In the corresponding pulse sequences, the synchronous atom is decelerated from 520 m/s to 365 m/s, 347 m/s and 333 m/s, corresponding to effective equilibrium phase angles of 30°, 45° and 60°, respectively. The corresponding loss of kinetic energy amounts to 23 cm^{-1}, 25 cm^{-1} and 27 cm^{-1}. The arrival time of the synchronous atom in the graphs is indicated by the vertical green lines. Black traces show the measured profiles; the gray traces that are shown as an overlay are obtained when the decelerator was not operated, i.e., the solenoids are all inactive but the permanent hexapole magnets are still present to focus the beam transversely.

The experimental TOF profiles are compared with profiles that result from three dimensional trajectory simulations. In these simulations, an initial beam distribution is assumed that closely resembles the He* pulse generated by the modified ELV. The resulting TOF profiles are shown in red, vertically offset from the measured profiles for clarity. The simulated profiles show good agreement with the experiment, both in relative intensity and arrival time of the peaks. However, it must be noted that the relative intensities are very sensitive to the chosen parameters of the initial He* pulse. By virtue of the supersonic expansion and discharge processes, these distributions are often not precisely known, and may vary from day to day. Nevertheless, the agreement obtained here, in particular regarding the overall shape of the TOF profiles and the predicted arrival times of the decelerated beam, suggests that the trajectory simulations accurately describe the motion of atoms inside the decelerator. No indications are found for unexpected loss of atoms during the deceleration process, or for behavior that is not described by the simulations.

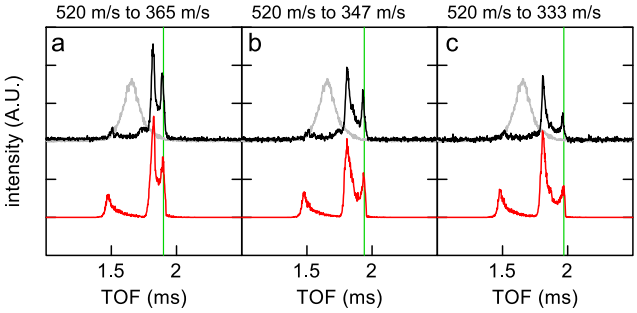

Figure 4. TOF profiles of He* exiting the Zeeman decelerator when the decelerator is operated in deceleration mode using an effective equilibrium phase angle of 30° (*a*), 45° (*b*) and 60° (*c*). Deceleration sequences were used to select an initial velocity of 520 m/s, resulting in the final velocities mentioned above each graph. Black traces are the experimentally obtained profiles, red traces show the profiles that result from numerical trajectory simulations. The gray traces show the TOF profiles that are measured when all solenoids are switched off. Vertical green lines indicate the arrival times of the synchronous atoms that are expected from the simulations.

The profiles presented in Figure 4 show more features than the decelerated packets alone. In particular, there is an additional decelerated peak in each of the graphs that is more intense but slightly faster than the decelerated packet. We use the three dimensional trajectory simulations to study the origin of this feature. In Figure 5, the longitudinal phase-space distributions are shown that result from these simulations at the entrance (upper panel), middle (central panel), and exit (lower panel) of the decelerator. The simulation pertains to the situation that results in the TOF profiles presented in Figure 4*a*, i.e., the decelerator is operated in deceleration mode with $\phi_0 = 30°$.

In these phase-space distributions, the grey contour lines depict the predicted trajectories considering the time-averaged Zeeman potential energy. The separatrix of the stable phase-space is highlighted with a cyan overlay. From this evolution of the longitudinal phase-space distribution, we can understand the origin of various pronounced features in the TOF profiles. The first peak in each TOF profile is a collection of the fastest particles in the initial beam distribution. These particles are hardly affected by the solenoids, and propagate to the detector almost in free flight. However, the part of the beam that is initially slower than the synchronous molecule is strongly affected by the solenoids. This part eventually gains in velocity relative to the decelerated bunch, resulting in an ensemble of particles with a relatively high density. This part arrives at the detector just before the decelerated He* atoms, resulting in the second intense peak in the TOF profiles of Figure 4. It is noted that this

peak appears intense because our decelerator is rather short, leaving insufficient time for the decelerated bunch to fully separate from the initial beam distribution. For longer decelerators, the part of the beam that is not enclosed by the separatrix will gradually spread out, and its signature in the TOF profiles will weaken.

The phase-space distributions that are found at the end of the decelerator may also be used to determine the velocity width of the decelerated packet of atoms. For the examples of Figure 5, these widths are about 25 m/s.

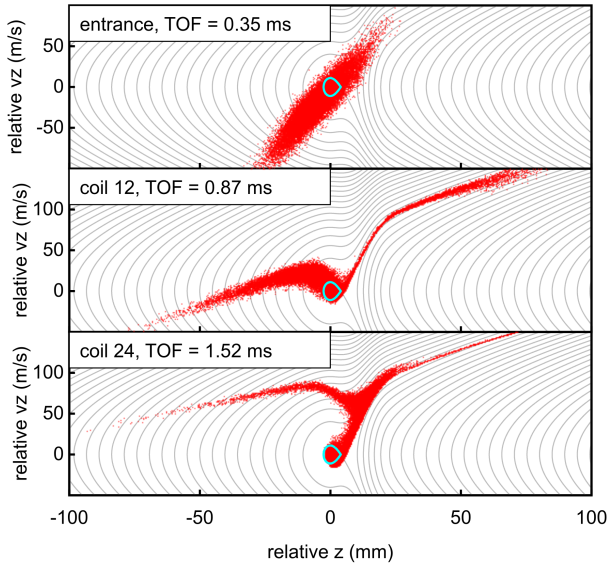

Figure 5. Longitudinal phase-space distributions of He* atoms during a deceleration sequence from 520 m/s to 365 m/s, obtained from simulations. The horizontal (vertical) axis shows the longitudinal position (velocity) relative to the synchronous atom. Each red dot represents a simulated He* atom. Grey contour lines show the expected trajectories derived from the averaged Zeeman potential energy, and the cyan contour shows the separatrix of the stable region in phase-space. The distributions are sampled at the time the synchronous atom enters the decelerator (top), when it arrived at solenoid 12 (middle) and solenoid 24 (bottom).

For completeness, we also measure a TOF profile when the decelerator is operated in acceleration mode. Figure 6*a* shows the TOF profile for the acceleration of He* atoms from an initial velocity of 560 m/s to a final velocity of 676 m/s. The simulated profile (red trace) shows good agreement with the experimental profile (black trace). Again, the vertical green line indicates the expected arrival time of the accelerated bunch. The sequence selects the fastest atoms in the beam, which is why no additional peaks are visible.

Finally, we study the performance of the decelerator in hybrid mode. This mode of operation allows for guiding of the beam through the decelerator at constant speed. In Figure 6*b* a TOF profile is shown when the decelerator is operated in hybrid mode and $\phi_0 = 0°$, selecting an initial velocity of 520 m/s. The simulated TOF profile (red trace) again shows good agreement with the experimental TOF profile (black trace), although the intensity ratios between the guided part and the wings of the distributions are slightly different in the simulations than in the experiment. This is attributed to the idealized initial atom distribution that are assumed in the simulations.

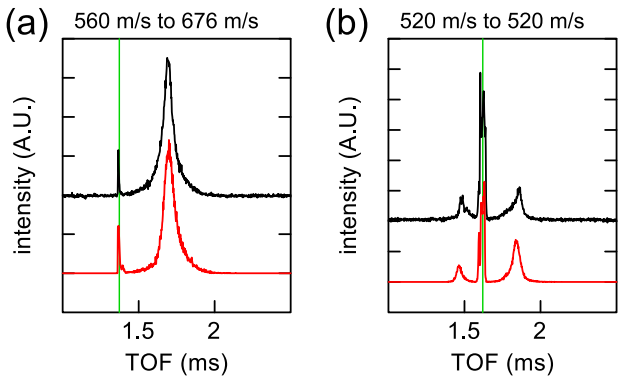

Figure 6. (*a*) TOF profile of He* accelerated by a multi-stage Zeeman decelerator from 560 m/s to 676 m/s. The black and red trace correspond to the experimental and simulated TOF profiles, respectively. (*b*) Experimental (black) and simulated (red) TOF profile when the decelerator operates in hybrid mode, guiding a bunch of atoms with mean velocity of 520 m/s. The vertical green lines depict the arrival time of the synchronous atom in the simulation.

B. Presence of metastable helium molecules

While our experiment is designed to decelerate He* atoms in the ^{3}S state, other types of particles may be created in the discharged beam as well. Specifically, formation of metastable He_2 molecules in the $a^3\Sigma$ state (from here on He_2*) is expected, as is also observed in the experiments by Motsch *et al.* that use a similar discharge source [4]. However, He_2* is indistinguishable from He* in our detection system. In order to probe both species separately, mass selective detection using a non-resonant laser ionization detection scheme is used. Ultra violet (UV) laser radiation with a wavelength of 243 nm is produced by doubling the light from an Nd:YAG-pumped pulsed dye laser running with Coumarin 480 dye, and focused into the molecular beam close to the exit of the decelerator. The resulting ions are extracted with an electric field of about 1 kV/cm and accelerated towards an MCP detector, where the arrival time of the ions reflect their mass over charge ratio.

We used this detection scheme to investigate the chemical composition of the beam that exits the Zeeman decelerator. In Figure 7, ion TOF spectra (i.e., the arrival times of the ions at the MCP detector with respect to the laser pulse) are shown. The black trace shows the

ion TOF spectrum if the beam of He* atoms is passed through the decelerator without operating the solenoids. The UV laser is fired at the mean arrival time of the beam in the laser ionization region. Two peaks are clearly visible corresponding to the expected arrival time of He^+ and He_2^+, confirming that indeed He_2 molecules are created in the discharge. There is about an 8:1 population ratio between He atoms and molecules in the neutral beam, assuming equal ionization and detection efficiency.

The green trace in Figure 7 shows the ion TOF spectra that is recorded when the solenoids are operated for a typical deceleration sequence similar to the ones used to generate Figure 4. This trace was taken when the UV laser selectively detects the decelerated part of the He* beam. Here, only He^+ is present in the ion TOF spectrum. Although He_2* has the same magnetic moment as He* and will thus experience the same force, the double mass of the molecule results in only half the acceleration. He_2* is therefore not decelerated at the same rate as He*, and will not exit the decelerator at the same time as the decelerated He* atoms. In conclusion, the Zeeman decelerator is quite effective in separating He* from the He_2*; the decelerated bunch only contains those species and/or particles in the quantum level for which the deceleration sequence was calculated.

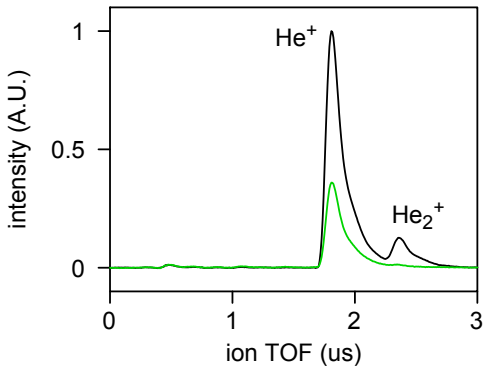

Figure 7. Ion-TOF spectra of ions created when UV radiation interacts with the He* beam that exit the Zeeman decelerator at various times. The black trace is taken for a beam that passes through the decelerator with inactive coils, while the green trace results from a Zeeman decelerated part of the beam.

Referring back to Figures 4 and 6 that were recorded without laser-based mass spectroscopic detection, one may wonder how the presence of He_2 molecules in the beam affect the recorded TOF profiles. Figure 8 revisits the measurement from Figure 4*a*, but taking also He_2 molecules into account with the appropriate ratio to generate the simulated TOF profile. The resulting TOF profile for He_2* molecules is shown by the green trace, and is seen to fill the part of the TOF that was under represented by the original simulations (indicated by the vertical green arrow for the experimental trace).

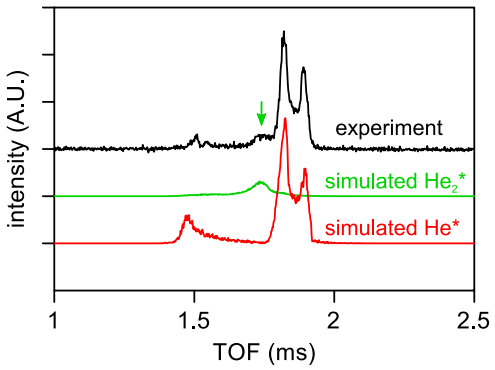

Figure 8. TOF profile from Figure 4*a* revisited. The experimental (black) profile is compared to simulated profiles for He* (red) and He_2* (green). The simulated signal of He_2* is scaled to 1/8 of the He* signal. Each profile is vertically offset for reasons of clarity.

IV. CONCLUSIONS AND OUTLOOK

We demonstrated the experimental implementation of a new concept for multistage Zeeman deceleration, that was introduced and described in the accompanying paper. We utilize a rather unconventional solenoid design that uses a thick copper capillary through which cooling liquid is circulated. The solenoid design allows for the switching of high currents up to 4.5 kA, using readily available and cheap low-voltage electronics components. Hexapole elements made from permanent magnets yield good results; if tunability of the transverse focusing forces is required, an optimized design of electromagnetic hexapoles will be needed.

The performance of the decelerator was experimentally tested using beams of metastable He atoms. Both deceleration, acceleration, and guiding of a beam at constant speed have been demonstrated. The experimental TOF profiles of the atoms exiting the decelerator show excellent agreement with the profiles that result from numerical trajectory simulations. Although the decelerator presented here only contains 24 solenoids, up to 60% of the kinetic energy of He* atoms that travel with an initial velocity of about 520 m/s could be removed.

The Zeeman decelerator presented here is mechanically simple, and can be built at relatively low cost. We are currently developing an improved version of the decelerator, that is fully modular, and that can be extended to arbitrary length. The modules can be connected to each other without mechanically disrupting the solenoid-hexapole sequence, while the housing design will allow for the installation of sufficient pumping capacity to maintain excellent vacuum conditions throughout the decelerator. Operation of the Zeeman decelerator consisting of 100 solenoids and 100 hexapoles at repetition rates up to 30 Hz appears technically feasible.

V. ACKNOWLEDGMENTS

The research leading to these results has received funding from the European Research Council under the European Union's Seventh Framework Programme (FP7/2007-2013/ERC grant agreement nr. 335646 MOLBIL). We acknowledge financial support from the Netherlands Organisation for Scientific Research (NWO). We thank Katrin Dulitz, Paul Janssen, Hansjürg Schmutz and Frédéric Merkt for stimulating discussions on Zeeman deceleration, solenoid focusing properties and current switching protocols.

[1] A. W. Wiederkehr, S. D. Hogan, and F. Merkt, Phys. Rev. A **82**, 043428 (2010).
[2] K. Dulitz, M. Motsch, N. Vanhaecke, and T. P. Softley, J. Chem. Phys. **140**, 104201 (2014).
[3] K. Dulitz, A. Tauschinsky, and T. P. Softley, New J. Phys. **17**, 035005 (2015).
[4] M. Motsch, P. Jansen, J. A. Agner, H. Schmutz, and F. Merkt, Phys. Rev. A **89**, 043420 (2014).
[5] N. Vanhaecke, U. Meier, M. Andrist, B. H. Meier, and F. Merkt, Phys. Rev. A **75**, 031402(R) (2007).
[6] S. D. Hogan, A. W. Wiederkehr, M. Andrist, H. Schmutz, and F. Merkt, J. Phys. B: At. Mol. Opt. Phys. **41**, 081005 (2008).
[7] E. Narevicius, A. Libson, C. G. Parthey, I. Chavez, J. Narevicius, U. Even, and M. G. Raizen, Phys. Rev. A **77**, 051401(R) (2008).
[8] Y. Liu, S. Zhou, W. Zhong, P. Djuricanin, and T. Momose, Phys. Rev. A **91**, 021403 (2015).
[9] E. Lavert-Ofir, L. David, A. B. Henson, S. Gersten, J. Narevicius, and E. Narevicius, Phys. Chem. Chem. Phys. **13**, 18948 (2011).
[10] A. Trimeche, M. Bera, J.-P. Cromiéres, J. Robert, and N. Vanhaecke, Eur. Phys. J. D **65**, 263 (2011).
[11] A. W. Wiederkehr, M. Motsch, S. D. Hogan, M. Andrist, H. Schmutz, B. Lambillotte, J. A. Agner, and F. Merkt, J. Chem. Phys. **135**, 214202 (2011).
[12] U. Even, J. Jortner, D. Noy, N. Lavie, and C. Cossart-Magos, J. Chem. Phys. **112**, 8068 (2000).
[13] L. Ploenes, D. Haas, D. Zhang, S. Y. T. van de Meerakker, and S. Willitsch, Rev. Sci. Instrum. **87**, 053305 (2016).